Borophene via Micromechanical Exfoliation

Sumit Chahal, Pranay Ranjan, Maithili Motlag, Sharma S. R. K. C. Yamijala, Dattatreya J. Late, El Hadi S. Sadki, Gary J. Cheng,* and Prashant Kumar*

Borophene, the lightest among all Xenes, possesses extreme electronic mobility along with high carrier density and high Young's modulus. To accomplish device-quality borophene, novel approaches of realization of monolayers need to be urgently explored. In this work, micromechanical exfoliation is discovered to result in mono- and few-layered borophene of device quality. Borophene sheets are successfully fabricated down to monolayer thickness. Distinct crystallographic phases of borophene viz. XRD study reveals crystallographic phase transition from rhombohedral to several other eigen phases of borophene. The role of the destination substrates is held crucial in determining the final phase of the transferred sheet. The exfoliation energy is calculated by density functional theory. Molecular dynamics simulations are used to simulate the exfoliation process. Heterolayers of borophene, with black phosphorene (BP) or with molybdenum disulfide (MoS_2) atomic sheets, are found to result in photoexcited coupling quantum states. Gold-coated borophene bestows promising anchoring capability for surface-enhanced Raman spectroscopy (SERS). Successful demonstration of the electronic behavior of micromechanically exfoliated borophene and excitonic behavior of borophene-based heterolayers will guide future generation devices not only in electronics and excitonics, but also in thermal management, electronic packaging, hydrogen storage, hybrid energy storage, and clean energy solutions.

1. Introduction

Borophene, the lightest elemental Dirac material capable of two-electron-three-center binding has intriguing crystallographic structures (β_{12} and X_3 being primary phases which are

metallic), is a new sensation in the flatland.[1–3] Incidentally, among various 2D materials, while boron nitride (BN) has large Young's modulus but compromised mobility, phosphorene and silicene have appreciable carrier mobility but compromised elastic behavior.[4] Graphene, considered the wonder material of this century fairs exceedingly well and its carrier mobility, as well as Young's modulus, are simultaneously high, which places it at a different pedestal.[5,6] However, e–h symmetry and spin symmetry in graphene result in insufficient signal/noise ratio in electronic as well as spintronic chips.[7] Borophene, being metallic in both β_{12} and X_3 crystallographic phases, also has excellent elastic strength and electronic mobility, which altogether places it at a significant pedestal among 2D materials. The evolution of borophene is expected to bring in new dimensions to 2D-material-based next-generation devices[8] (see the schematic plot in **Figure 1**a for the comparative presentation of ln (mobility) vs Young's modulus for various 2D materials).[9–13] Anisotropic atomic ordering results in enhanced electronic mobility ≈1.82×10^6 cm^2 V^{-1} s^{-1}, Young's modulus ≈398 N m^{-1}, and thermal conductivity along atomic ridgelines.[14,15] In particular, for flexible electronic as well as spintronic chip applications, high electron mobility and Young's modulus are desirable simultaneously and borophene

Dr. S. Chahal, Dr. P. Ranjan, Prof. P. Kumar
Department of Physics
Indian Institute of Technology Patna
Patna, Bihar 801106, India
E-mail: prashantkumar@iitp.ac.in

Dr. P. Ranjan, Dr. E. H. S. Sadki
Department of Physics
College of Science
United Arab Emirates University
Al-Ain, UAE

Dr. M. Motlag, Prof. G. J. Cheng
School of Industrial Engineering
Purdue University
West Lafayette, IN 47907, USA
E-mail: gjcheng@purdue.edu

Dr. S. S. R. K. C. Yamijala
Department of Chemistry
Indian Institute of Technology Madras
Chennai 600036, India

Dr. D. J. Late
Centre for Nanoscience and Nanotechnology
Amity University Mumbai
Mumbai, Maharashtra 410206, India

Prof. G. J. Cheng
School of Materials Engineering
Purdue University
West Lafayette, IN 47907, USA

Prof. G. J. Cheng, Prof. P. Kumar
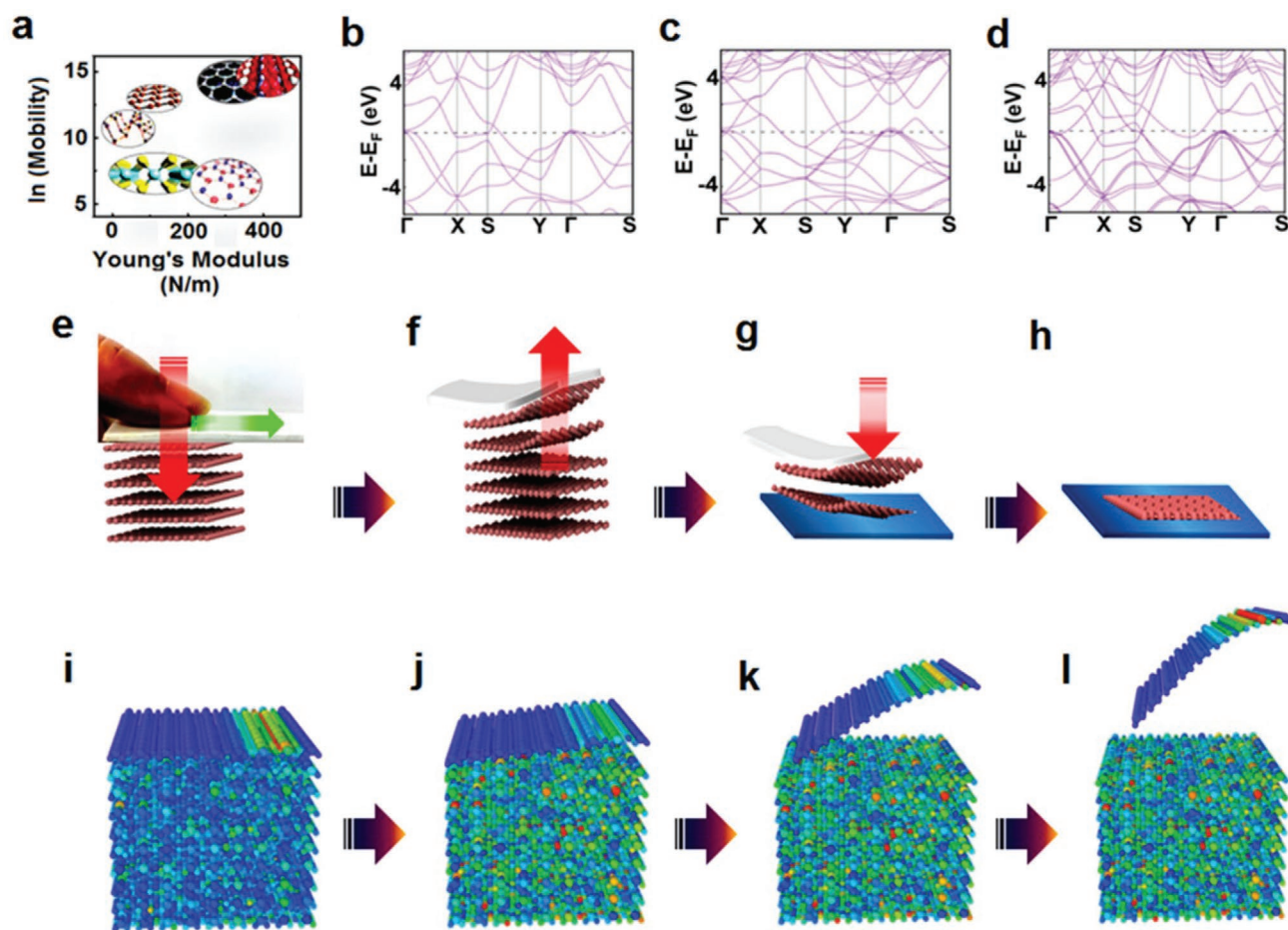Birck Nanotechnology Centre
Purdue University
West Lafayette, IN 47907, USA

Figure 1. Molecular dynamics simulation for borophene exfoliation. a) Schematic diagram representing a comparative plot of ln (mobility) versus Young's modulus for various 2D materials staring from having low value of ln (mobility) of boron nitride (BN), molybdenum disulfide (MoS$_2$), black phosphorene (BP), arsenene (As), graphene (Gr), and borophene (B) on the top. b–d) Density functional theory (DFT) band structure for β_{12} phase of borophene for mono-, bi-, and tri layers. As the number of layers gradually increases from monolayer to trilayer, due to enhanced interlayer coupling, in-plane interactions will be curtailed resulting in crystallographic symmetry modulation and eventually impacts electronic band structure as well, as is evident from Dirac point shift from Γ to other k-values. This brings in significant modulation to the energy landscape for borophene. Moreover, the density of energy states also changes with the rise in number of layers. Thus, electronic behavior of borophene distinctly changes with the number of layers. e–h) Various steps of micromechanical exfoliation of borophene. e) Double-sided foam tape is pressed against the crystal of the boron to exfoliate the boron layers via giving normal (red arrow) and shear (green arrow) forces. f) Peeling off the layers from the crystal. (g) Exfoliated layers are pressed against the substrate (SiO$_2$). h) Finally, the bottom layer of exfoliated borophene is transferred to the substrate. i–l) Various stages of micromechanical exfoliation of monolayer borophene from bulk boron crystal carried out by MD simulation over 70 ps.

fits extraordinarily well in that role vis-à-vis other existing 2D materials (see Figure 1a).[9–14,16] Ridgelines can act as excellent anchors for molecules and therefore the simplistic device can deliver ultrasensitive molecular sensing. Apart from its applications in strain and light sensing, borophene is tipped to be excellent in terahertz plasmonic waveguiding.

Experimental realization of borophene has earlier been reported by atomic layer deposition (ALD),[17] molecular beam epitaxy (MBE),[18] and chemical vapor deposition[19,20] over a silver surface. The irony was that the crystal structure of silver substrate was held responsible for the very crystallization of borophene. Ambiguity stemmed from a myth that boron crystal in its bulk is not a van der Waals crystal and therefore it cannot be exfoliated. Recent reports on exfoliation of borophene attained by sonochemical as well as modified Hummer's approach have finally broken the myth completely.[21,22]

However, exfoliation of borophene employing solvents or chemical reagents results in defects/functionalities and it also fragments the sheets. Thus, on the one hand, ultrahigh vacuum (UHV) conditions make the cost sky-high and the electronic behavior of the substrate grown borophene has the effect of the substrate inherently present in it, on the other hand, liquid-phase exfoliated borophene might have solvent-originated surface functionalities. For practical realization of ultrasensitive borophene-based devices and sensors which have been a dream for quite some time, one needs to have large area crystals (substrate-independent, if feasible), devoid of any defects or functionalities to realize and exploit its intrinsic physical and chemical behavior. This has been a technological bottleneck in the development of several frontline applications of borophene. Incidentally, micromechanical direct exfoliation of borophene has never been accomplished to date due to several practical

**ADVANCED
SCIENCE NEWS**

www.advancedsciencenews.com

**ADVANCED
MATERIALS**

www.advmat.de

challenges including misunderstanding of the crystal structure of boron, and therefore, if at all it can be attained, would pave the way for the fabrication of future generation borophene-based ultrasensitive devices and sensors. Currently, a thorough in-depth theoretical understanding of the exfoliation of borophene has not yet been established.

Gauging the urgency, we have employed micromechanical exfoliation of borophene directly from boron crystal onto thermally oxidized silicon (Si/SiO_2) as well as indium tin oxide (ITO). Exfoliated atomic sheets were characterized by a host of microscopy tools such as field-emission scanning electron microscopy (FESEM), atomic force microscopy (AFM), and transmission electron microscopy (TEM) as well as spectroscopic tools such as Raman spectroscopy, X-ray photoelectron spectroscopy (XPS), and Fourier transform infrared (FTIR) spectroscopy. Exfoliation energy for borophene was computed employing density functional theory (DFT). DFT band structure for β_{12} phase of borophene for mono-, bi-, and trilayers are shown in Figure 1b–d. A larger number of layers exhibit enhanced interlayer coupling, giving rise to poor in-plane interactions which eventually result in altered crystallographic structures. The Dirac point shifts to other k-indices and modulation in dispersion behavior (nature of dispersion curve) are witnessed as a result. A clear distinction is observed for band locations with respect to the Fermi level. The density of states is altered with the gradual increase in the number of layers.[21] Molecular dynamics (MD) simulation was carried out to explore the details of the exfoliation process. Transferred borophene was intentionally oxidized to understand the oxidation issues in practical devices and was tested for chemical phase purity by X-ray diffraction (XRD), Raman spectroscopy, as well as FTIR spectroscopy. The effects of oxidation of borophene on electrical behavior were also investigated. To explore excitonics in borophene-based potential heterolayered devices, we fabricated an interface of borophene separately with those of 2D semiconductors such as black phosphorene (BP) and molybdenum disulfide (MoS_2). Heterolayers were chemically identified from Raman fingerprints and excitonics in a heterolayered system explored by laser-excited photoconductivity measurements in out-of-plane geometry. To demonstrate surface-enhanced Raman spectroscopy (SERS)-based molecular sensing application, gold-coated borophene was used as a SERS anchor for methylene blue (MB).

2. Micromechanical Exfoliation

Even though the myth about the crystal structure of boron in its bulk form has continued to date, in our quest to obtain borophene in its pure form by micromechanical exfoliation without the usage of any chemical reagent, we indeed attained success. The idea of exfoliation primarily involves the application of vertical pressure which helps the top borophene layer adhesion with the double-sided foam tape used (see Figure 1e–h). On the one hand, double-sided foam tape has strong polymer adhesive which helps in improved adhesion of borophene layer with the tape, and on the other hand, the thick foam helps in enhanced manual vertical pressure transfer. Micromechanical exfoliation was simulated for the β_{12} phase and was found to

result in changes in the energetics (local temperature) of atoms in the exfoliated sheet as well as the remaining layers. Exfoliation causes strain in the system. Various stages of exfoliation simulated up to 70 ps are shown in Figure 1i–l. Potential energy variation from −2109 to −2086 eV causes the loss of 23 eV for the top layer exfoliation of borophene in a period of 70 ps, as shown in Figure S1 (Supporting Information). Digital camera image along with an optical image of the parent crystal exhibits facets with certain texture on its surface (see **Figure 2**a,b). Raman spectrum acquired on its surface exhibited distinct Raman peaks at 829, 946, 1172, and 1196 cm^{-1} (see Figure 2c). Various steps of exfoliation have been demonstrated through digital images (see Figure 2d). The double-sided tape works as a cushion layer. When the adhesion (between the adhesive surface of the tape and the top layer of boron crystal) breaches van der Waals cohesive force between the top layer and the stack of the remaining layer, exfoliation takes place. Optical images of borophene sheets have folds and bend at the edges (see Figure 2e,f). XPS studies on exfoliated borophene sheets, especially the absence/negligible presence of oxygen shoulder in B 1s stretch are interesting to note (see Figure 2g,h). We could obtain borophene sheets of few micrometer lateral dimensions of transferred sheets on SiO_2/Si substrate; however, they were relatively thicker, as evident from the straightened stiff sheets (see Figure 2i–l). Thus, successful micromechanical exfoliation and transfer of borophene are demonstrated on SiO_2/Si substrate. AFM imaging in 3D view further reveals the 2D nature of transferred borophene along with the corresponding Raman spectra (see **Figure 3**a–o). Line profile captured for various numbers of successive peeling steps and subsequent transfers exhibit flat hat-shaped features which are characteristic of 2D materials and the thicknesses of the transferred sheets are 5, 9, 13, 21, and 41 Å which correspond to monolayer, bilayer, trilayer, 5 layers, and 10 layers, respectively (see Figure S2 in the Supporting Information for 2D as well as a 3D view of AFM images). It was observed that the first layer thickness is 5 Å and further layers were 4 Å each. Such observation is possibly due to strong B–B cohesive force than B–SiO_2 adhesive forces. We carried out detailed AFM imaging of transferred sheets and we conclude that several sheets of marginal thicknesses and lateral dimensions (see Figure S3 in the Supporting Information) have been witnessed which proves exfoliation down to monolayer thickness. While bulk boron crystal exhibits XRD peaks resembling preferentially with trigonal/rhombohedral ($R\overline{3}m$) structure (JCPDF 00-031-0207) (see Figure S13 in the Supporting Information).[23] Even the tetragonal symmetry phase has some peaks matching with the XRD peaks obtained for the crystal used in the present research. Moreover, rhombohedral and hexagonal lattice symmetries find a few peaks in common, in general, not identical though. Exfoliated sheets however exhibited signature of not only from parent crystal but new XRD peaks were also observed, which attests to structural changes during exfoliation. Higher interlayer coupled boron sheets upon exfoliation would acquire structural configurations favoring energy minimization. It so happens with borophene that its several possible crystallographic phases have closed by the energy of formation, this brings in another interesting aspect, as to which final structure it will assume. The role of its interaction with the final destination substrate, therefore, emerges in the
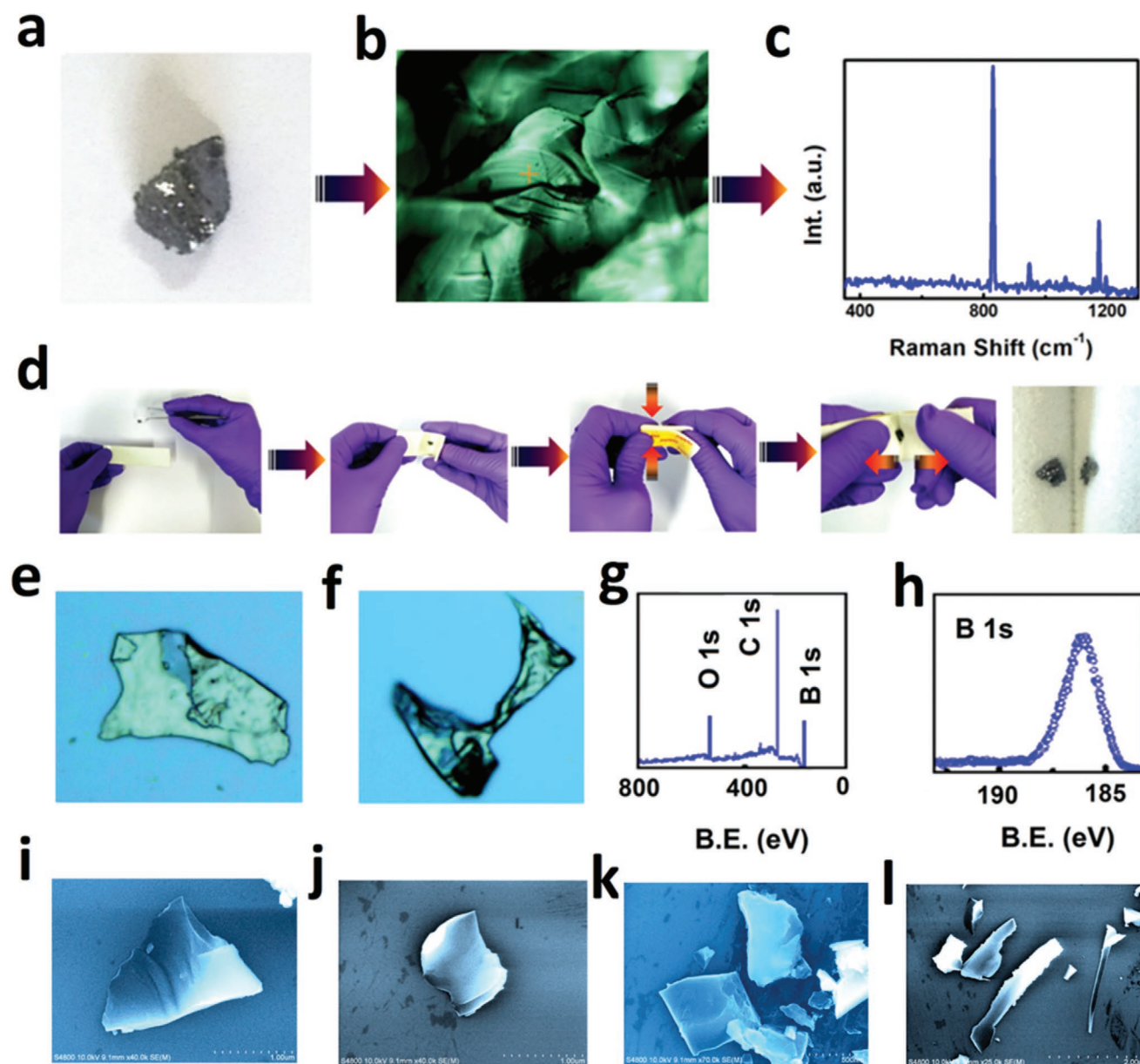
Figure 2. Micromechanical exfoliation. a) Camera image of borophene crystal. b) Optical image of borophene crystal. c) Raman spectrum acquired on bulk crystal exhibits distinct Raman peaks at 829, 946,1172, and 1196 cm^{-1}. d) Digital images of various steps of micromechanical exfoliation of borophene using double-sided foam tape. e,f) Optical image of exfoliated borophene transferred onto SiO$_2$/Si substrate. g,h) XPS survey spectrum of borophene along with B 1s spectra. i–l) FESEM images of exfoliated borophene having a lateral dimension of few micrometers.

choice of the phases it will assume and hence also in its atomic structure determination. It should be noted that new peaks in exfoliated sheets get reinforced when undergone through further exfoliation steps. Interlayer coupling loosens upon exfoliation and thus individual layers get the necessary freedom to reorient/reconstruct their structure into energetically favorable Eigen structures. The sequential and systematic Raman study of exfoliation in the present research hints at modulation of vibrational modes which vindicates structural transitions.

Raman fingerprints of borophene suggest the presence of primarily β_{12} phase along with some signature of stripe (X$_3$) phase of borophene. Mixed phases (β_{12} and X$_3$) are observed

at 10 and 5 layers. Relative Raman intensity has changed when sheets are thinned down from 10 to 5 layers (peaks located at 357, 456, 623, 679, 811, 1086, 1235 cm^{-1} (compare 3rd and 4th peaks at the middle and last two peaks))[21] (see Figure 3c,f). Some Raman modes are thus suppressed and other ones are reinforced as the interlayer coupling is altered (lowered when thinned down). When only three layers remain, β_{12} signature is exclusively attained (peaks at 235, 304, 485, 681, and 747 cm^{-1})) (see Figure 3i). As we lower down the thickness to bilayer and monolayer, the Raman peaks were observed at 375, 725, and 1068, 370 and 1060 cm^{-1}, respectively. Observed peaks for the monolayer are the dominant peaks of the β_{12} phase of
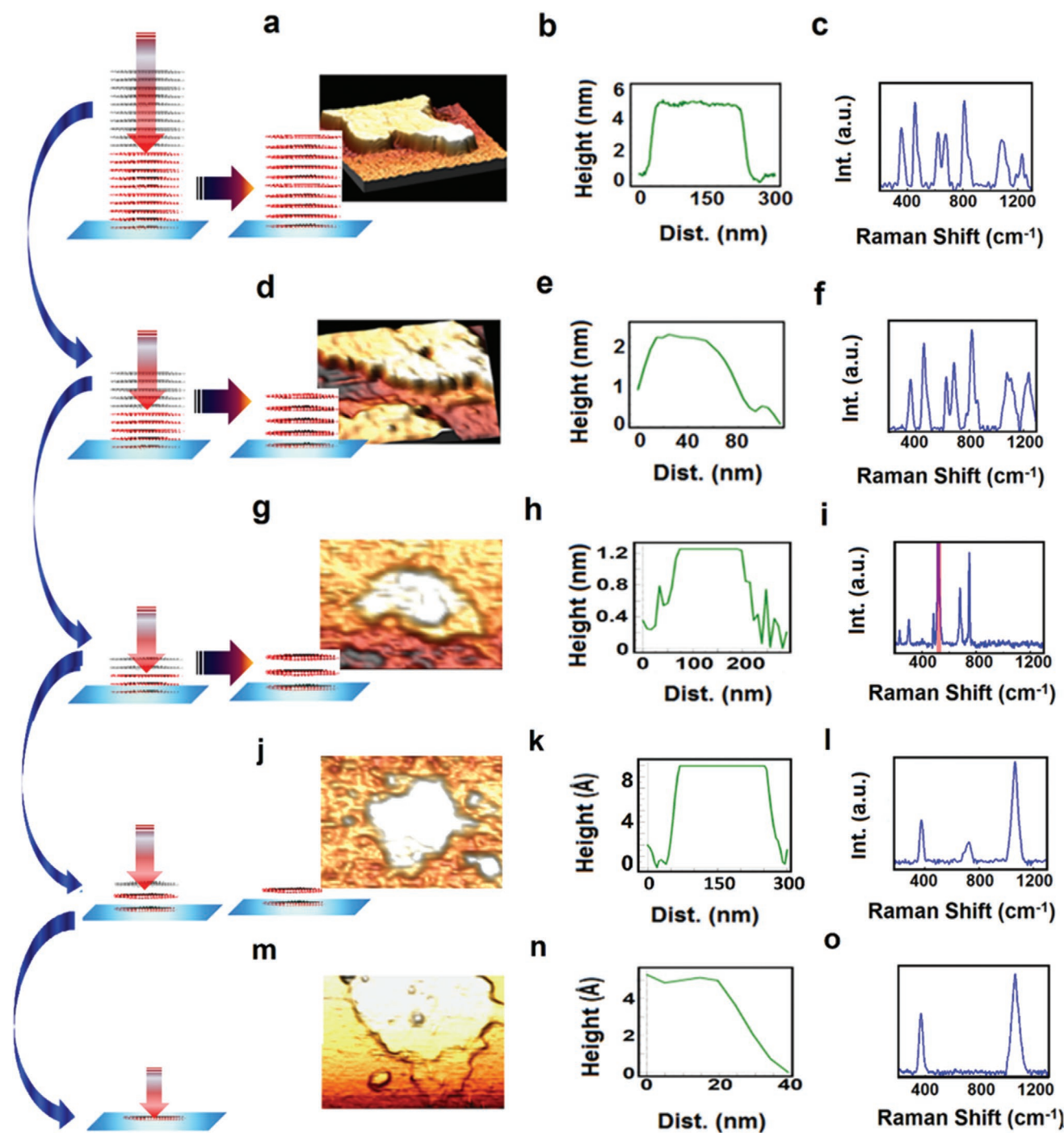
Figure 3. Demonstration of layer transfer and characterization of borophene. Micromechanical transfer of borophene atomic sheets is done in a sequential manner. Successive peeling steps reduce the remaining layer thickness attached with the foam tape. When placed on a desirable substrate and adequate vertical pressure is applied onto it against the substrate, layers in contact with the substrate remains attached with it. Remaining layers on tape are again pressed on another substrate and thus thinner and thinner sheets are attained. Thus, a desirable number of layers of borophene can be accomplished via micromechanical exfoliation in a tunable manner and on the substrate of one's choice. Demonstration of micromechanical transfer: a,b) AFM image and line profile of ≈10 layers, d,e) AFM image and line profile of ≈5 layers, c,f) Raman spectrum acquired for ≈10 layer borophene sheet exhibits peaks at 357, 456, 622, 677, 814, 1087, 1227 cm^{-1} and for 5 layer borophene at 363, 462, 630, 683, 819, 863, 1075, 1104, 1241 cm^{-1} (both β_{12} and stripe (X_3) phase Raman signatures are witnessed), g,h) AFM image and line profile of ≈3 layers, i) Raman spectrum acquired for ≈3 layer borophene sheet (only β_{12} Raman signatures are witnessed), j,k) AFM image and line profile of bilayer borophene, l) Raman spectrum of bilayer borophene having peaks at 370 and 1060 cm^{-1}, m,n) AFM image and line profile of monolayer borophene, o) Raman spectrum having peaks at 375, 725, and 1068 cm^{-1}.

**ADVANCED
SCIENCE NEWS**

www.advancedsciencenews.com

**ADVANCED
MATERIALS**

www.advmat.de

borophene (see Figure 3l,o). This hints at the preferential formation of β_{12} phase in monolayer, bilayer, and trilayer borophene (see Figure 3c,f,i,l,o and Figure S4 in the Supporting Information for details).[21,22,24]

The electron-deficient character of boron drives to ample number of bonding configurations starting from two-center two-electron bonds up to seven-center two-electron bonds.[25] Multicenter polymorphic configurations lead up to 16 bulk allotropes of boron (see Figure S5 in the Supporting Information), a variety of lattice configurations that lie within a narrow range of energies set apart by hexagonal holes make 2D boron adopting a structure depending on the substrate compared to other 2D materials[3,26–28] (see Figure S6 in the Supporting Information). The clustering tendency of boron atoms results in polymorphic nature and thus the realization of pure phase in 2D crystal becomes experimentally challenging. Even though it has been realized by various UHV methods of fabrication, e.g., ALD and MBE, however, it has been established that substrates predominantly determine crystal structure. There has long been a belief that without the activation by adequate substrate with matching crystal structure supporting crystal growth of its lattice, borophene crystal growth cannot be realized. This myth was broken by the realization of freestanding borophene earlier. However, the direct transfer of borophene from the parent crystal to the substrate has never been experimentally realized. TEM has been carried out to explore and distinguish various crystallographic configurations. The TEM image exhibiting 2D sheets as well as atomic stripe has been zoomed-in step by step (see **Figure 4**a,b) to demonstrate the atomic configuration in high-resolution TEM (HRTEM) image in Figure 4c, which further vindicates successful transfer of a few mono- and multilayered borophene. To dig details, zoomed-in versions of images in two different locations were analyzed and atomic arrays could be visualized along with the corresponding atomic structures (sections 1 and 2 in Figure 4c and 3D imaging of both sections in Figure 4d,e). Fast Fourier transform (FFT) obtained for marked area exhibits a central array of bright dots and subsidiary arrays with relatively dimmer dots in all the three zoom-in locations. Therefore, it was imperative to obtain atomic profiles along with the atomic array and normal to it to vividly establish the atomic ordering in fabricated borophene sheets. Interestingly enough though, along with the array, we could see the periodicity and along normal direction, we could observe bright peaks corresponding to atoms placed at higher and dim peaks corresponding to atoms situated at depth (red line) (see line profiles and FFT in Figure 4f,g). Thus, atomic profiles along with FFT patterns for Figure 4f suggest anisotropic arrays of atoms constructing ridgelines separated by an array of atoms situated at depth. HRTEM acquired in another area has altogether different atomic arrangements, i.e., intertwined atomic arrays and all atomic arrays had mostly bright peaks (see Figure 4e). Strain-driven ripple-like features have been witnessed giving rise to stripes (atomic clusters) (see Figure 4g). The average distance between atoms along ridgelines in Figure 4d was found to be 0.45 nm (distance between two bright atoms), in a direction normal to the ridgeline was 1 nm (see Figure 4f). However, between two ridgelines, arrays lying lower were also witnessed just midway between the ridgelines (see Figure 4f line profile (red)). TEM image of a large

area of borophene with a zoomed-in image having sharp edges are expected to be few monolayer (see Figure 4h,i). In between two bright linear arrays of atoms (ridgelines), two low-lying arrays of atoms are situated, which is the signature of the β_{12} ridgeline phase of borophene (see Figure 4j, for large area see Figure S7 in the Supporting Information). Inset FFT exhibits a linear array of bright dots. The average interatomic distance along the ridgeline was almost uniform throughout and it was 0.35 nm. In the normal directions, it varied. Low lying atoms come close up to ≈0.18 nm and they keep a distance ≈0.28 nm from ridgeline atoms (sees Figure 4k). TEM images of other regions probably seem to be mono- or bilayer, as is apparent from the high electron transparency, and visibility of its edge (see Figure 4l). HRTEM image (Figure 4m) corresponds to β_{12} phase and marked red region was then zoomed-in. As can be seen in Figure 4n, intertwining arrays of atoms were witnessed. The average interatomic distances at the splitting and overlapping atoms arrays were 0.26 and 0.535 nm, respectively (see Figure 4o).

Atomic structures observed in the direct transfer of borophene are distinctly different from the anisotropic phase of sonochemically exfoliated borophene reported earlier;[21] where three atomic arrays were witnessed lying lower in between the atomic arrays lying higher. The presence of ripple-like features as observed in HRTEM images may evolve due to local strain or Moire's patterns (which arise due to interlayer coupling when two consequent layers are inclined at some angles). The anisotropic phase is recognized in the literature as the β_{12} phase and the other isotropic phase as X₃. However, when we compare our results in the present direct transfer technique vis-à-vis those for sonochemical as well as for modified Hummer's technique[21] and also with those reported via ALD[17] and MBE[18] techniques, we conclude that crystallographic phases in borophene arise due to atomic interactions and available local residual strain. Substrates on which borophene is transferred would surely determine local strain, especially for monolayers as substrate atoms would interact with atoms in adhering borophene layer. The number of atoms per unit area is an excellent parameter to distinguish two distinct crystallographic structural phases for atomic sheets and we obtained 20 and 24 nm^{-2} for sections 1 and 2, respectively. In contrast to the present values of areal density for direct transfer technique, the molecular beam epitaxy technique had yielded 34.6 nm^{-2}.[18] It should be noted that in substrate supporting the growth of borophene, the number of boron atoms packed in a particular area is determined by the substrate–boron interaction, external parameters such as temperature, pressure, etc., would also impact the atomic packing in MBE/ALD or vapor phase growth. Even FFT patterns obtained for these phases exhibit distinguishable features. While in section 1, bright dots in the central line along with equidistant atoms (orderliness) are observed, clustering is profound in section 2. Understanding very interesting strain-driven emerging crystallographic structures will be crucial to tap promising applications of borophene. Central bright dots in FFT is a common feature in all two sections, however, subsidiary arrays of small dim dots have distinct features. Thus, these crystallographic phases observed in the direct transfer technique are distinct. The number of layers, interlayer distances, sliding displacements, and twist angles apart from the
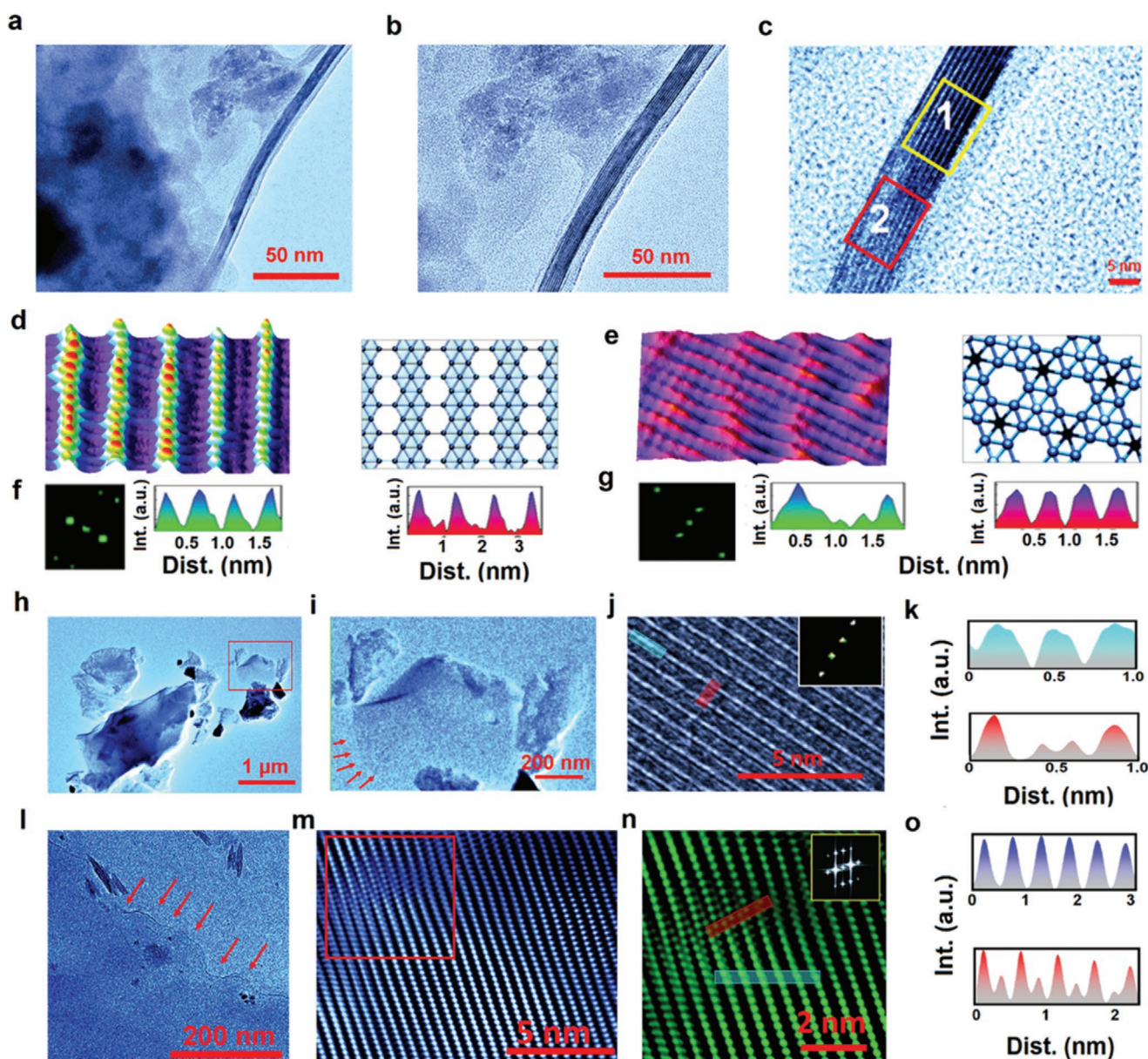
**ADVANCED
SCIENCE NEWS**

www.advancedsciencenews.com

**ADVANCED
MATERIALS**

www.advmat.de

Figure 4. HRTEM microscopy of exfoliated borophene. a,b) TEM images of exfoliated borophene sheets along with stripes of atoms at the edges. c) HRTEM image of atomic stripe bestows strain-mediated borophene phase as well. d,e) HRTEM images 3D view showing ridgeline phase Section 1 and interlinked phase section 2 of Figure 3c along with schematic atomic structures. f,g) FFT pattern and atomic line profile along the ridgeline (green) and normal to it (red) lying below are corresponding to sections 1 and 2, respectively. h,i) TEM image of another region of exfoliated borophene and the zoomed-in region marked by red boundary has sharp edges which hint at monolayer or few monolayers. j) HRTEM image with clearly visible ridgeline phase (β_{12}) along with its schematic atomic structure (inset FFT pattern). k) Atomic line profile of (j) along two directions exhibits average interatomic distances were 0.35 and 0.179 nm marked by cyan and red color lines, respectively. l) TEM image of large size flat borophene seat over the substrate SiO_2. m,n) HRTEM images along with the zoomed-in image with clearly visible outward and inward atoms. o) The average interatomic distances at two locations marked in (n) were 0.535 and 0.260 nm (correspond to marked red line).

substrate–borophene interactions would eventually determine the evolution of crystallographic phases.

A variety of crystallographic configurations have thus been witnessed in HRTEM imaging which arise due to the polymorphic character of borophene.[29] Several 2D materials exhibit phase transition from hexagonal planar phase (for 1–3 layers) to locally 3D protruded/ridgeline phases (>3 layers) with the increase of thickness. Unlike graphene, which is famous for

sp^2-hybridized hexagonal structure, borophene seems to lack sp^2-hybridized flat hexagonal structure (even if it is found locally, it is limited to a very small area). Thus, it is true that borophene is not an energetically stable flat atomic sheet. To minimize energy, therefore, defects such as periodic vacancies form an array of atoms that come above the usual plane or a combination of vacancies and protruded atoms. Theoretical crystallographic phases in fact can alter from what is observed

**ADVANCED
SCIENCE NEWS**

www.advancedsciencenews.com

**ADVANCED
MATERIALS**

www.advmat.de

experimentally. Destination substrate on which it is transferred has a big role as substrate–boron atom interactions play a huge role in the adhesion of borophene. Thus, the transfer of borophene can potentially alter its atomic structure too. Even though the crystallographic phases with varying atomic configurations are close in energy, they have distinct electronic structures. For example, in contrast to graphene, which has in-plane chemical bonding, borophene exhibits out-of-plane chemical bonding and periodic vacancies. Such atomic rendering would result in restricted electron flow in one direction and free flow in the ridgeline direction, bringing in anisotropic mobility. Similarly, anisotropic mechanical behavior is expected too.

3. Calculation of Exfoliation Energy

The direct transfer of borophene crystals on substrates is desirable for future generation device fabrication. However, at the core of it, the physicochemical processes involved in exfoliation are crucial. Boron is electron deficient, and therefore in most of its compounds, it forms two electrons three center binding.[1] Such bindings help share electrons and this is the reason for its tendency of forming clusters such as the β_{12} phase of borophene. β_{12} phase has 6 atoms surrounding a central atom and to efficiently share electrons, the central atom goes out-of-plane and this is the reason for ridgeline formation. These ridgeline formations help accommodate a greater number of atoms and their binding is enhanced. This enhanced binding is limited to the ridgeline direction only and therefore, one expects anisotropic elastic behavior. Carbon in graphene lattice is more stable than boron in borophene lattice as there is a greater number of atom sharing of the available electron. This is why interlayer coupling in borophene is better than that of graphene. Competition between cohesive forces among boron–boron atoms and adhesive forces among boron–carbon atoms would in particular determine whether exfoliation of the top layer of borophene would occur or not. On a similar note, adequate adhesion between boron to the target substrate would ensure successful borophene transfer. During the practical exfoliation process and transfer, pressure is not uniform and every atom does not respond as a single unit and thus local strain arises. To understand and appreciate the exfoliation process better, we carried out DFT to calculate exfoliation energy. From our ab initio calculations, we obtained the exfoliation energy of the borophene layer as 19.6 meV Å^{-2} for Perdew–Burke–Ernzerhof (PBE) functional (see Table S1 in the Supporting Information for detailed results with a different number of k-points) and −23.6 meV Å^{-2} using the Hyde–Sauceria–Ernzerhof (HSE) functional (see Table S2 in the Supporting Information) calculated over 14.8 Å^2 area of borophene. The reason behind the higher exfoliation energy of borophene can be traced to excellent binding in borophene crystal vis-à-vis other 2D materials (see Figure S8 in the Supporting Information).[30] Moreover, molecular dynamics simulation was also carried out to have a glimpse of generated strain profile. Interactions between top layers of borophene are stronger as compared to interlayer interactions for borophene for layers deeper in the bulk and similar behavior in 2D materials was also reported by Manimunda et al. for 2D materials.[31] Borophene as an emerging material for future generation

devices needs to be integrated into silicon and therefore, it is necessary to ascertain its lamination strength on to the substrate. Delamination of single- and bilayer borophene has been simulated by MD (see Figures S9 and S10 in the Supporting Information). Comparison of potential energy variation in time for mono- as well as bilayer borophene upon the process of delamination has been made (see Figure S11 in the Supporting Information). More negative potential energy was registered for the borophene–silicon system than in the borophene–boron system, this suggests that adhesion to the substrate is strong enough and borophene-based devices can be integrated into a silicon chip.

4. Thermal Oxidation Effect

Even though 2D materials are a new class of materials with interesting quantum mechanical behavior, structural stability and oxidation resistance are crucial for applicability point of view.[32,33] Borophene has not been explored much in detail and one of the reasons has been the illusion that it may instantly oxidize in ambient conditions, especially in humid conditions. To resolve this, we intentionally oxidized transferred borophene and analyzed it (see **Figure 5**a, schematic of borophene and borophene oxide). The deficiency of electrons makes it difficult to control the degree of oxidation in borophene, therefore, various borophene oxide configurations may form (e.g., BO, B_2O, B_4O, B_5O, B_7O, B_8O, etc.) (see Figure S12 in the Supporting Information).[34,35] Distinguishable Raman signatures of both borophene and borophene oxide are shown (see Figure 5b,c, respectively). FTIR stretches corresponding to oxygen functionalities (epoxy and other oxide forms) were observed for the borophene oxide sample obtained via thermal oxidation (see Figure 5d). XRD patterns of the borophene sample and the oxide sample obtained upon thermal treatment vividly distinguish their chemical identity (see Figure S13 in the Supporting Information). Interestingly, electrical conductivity in intentionally oxidized borophene was in nanoamperes, while it was thousands of times more in devices made up of borophene samples via direct transfer (see Figure 5e). Lack of oxide signals in various spectroscopies, as well as dramatically enhanced electrical signal strength for transferred borophene layers as compared to those for intentionally oxidized borophene, establishes the quality of borophene crystal obtained in this research. The real-life application of molecular sensing via SERS using borophene as an anchoring platform has tremendous capabilities. The Raman peaks for MB anchored upon gold-coated borophene are observed at 455, 606, 677, 800, 905, 957, 1033, 1162, 1308, 1395, 1430, 1512, and 1635 cm^{-1} (see Figure 5f). Significant enhancements in Raman signals of methylene blue were observed when anchored upon gold-coated borophene transferred over SiO_2 substrate with respect to molecules directly transferred on the gold-coated substrate.

5. Borophene-Based Heterolayers with Black Phosphorene and MoS$_2$

Recent developments on 2D-material-based heterolayered devices have gained popularity due to their wide range of

**ADVANCED
SCIENCE NEWS**

www.advancedsciencenews.com

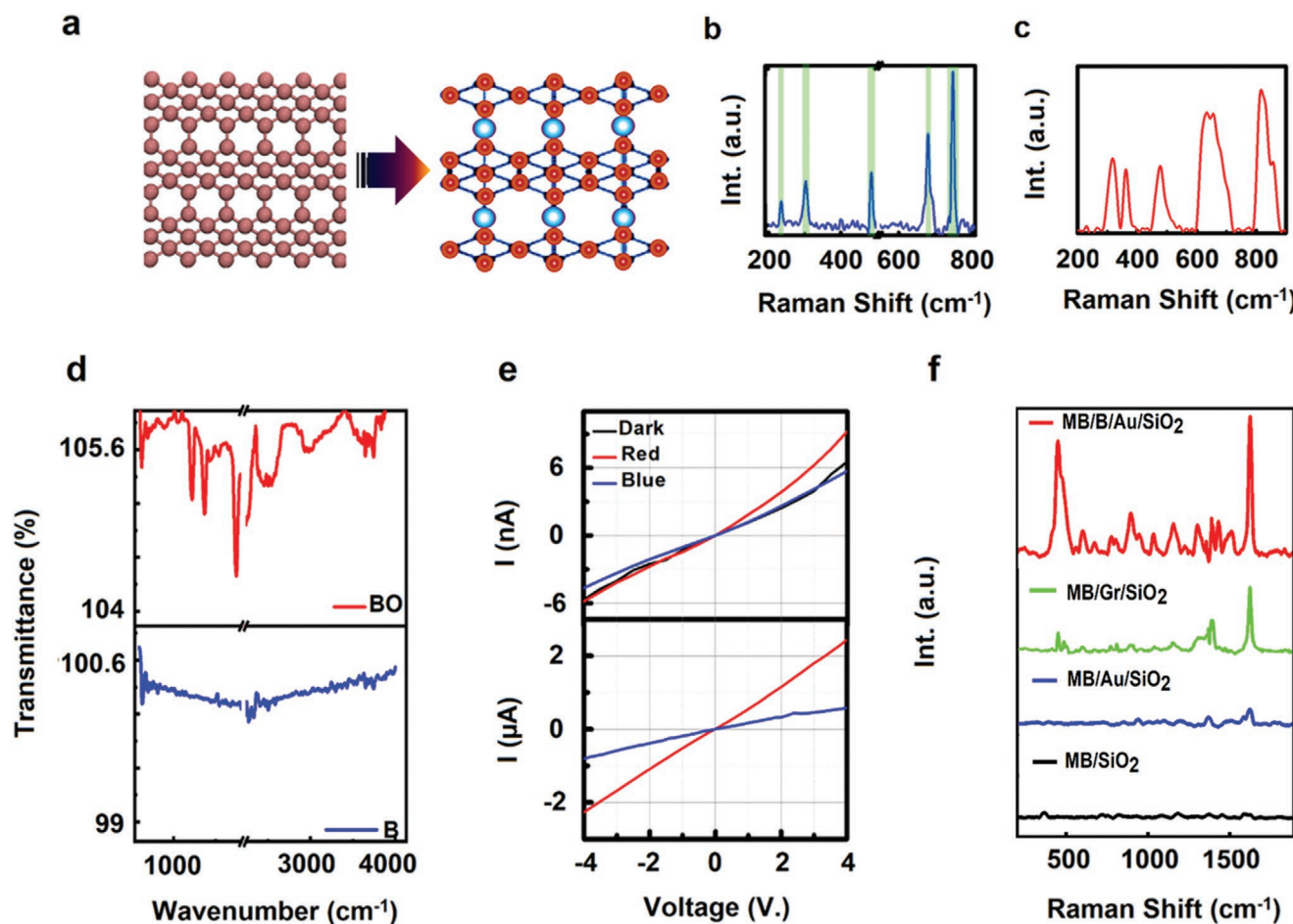**ADVANCED
MATERIALS**

www.advmat.de

Figure 5. Borophene and borophene oxide. a) Schematic atomic diagram of borophene and borophene oxide. b,c) Raman fingerprints of borophene and borophene oxide. d) Comparative plot of Fourier transform infrared (FTIR) spectroscopy of borophene (blue) and borophene oxide (red). e) Current versus voltage (*I–V*) and photoconductivity (PC) behaviors of borophene (lower plot) and borophene oxide (upper plot). f) Surface-enhanced Raman spectroscopy (SERS) of methylene blue (MB) over SiO_2, Au/SiO_2, and $B/Au/SiO_2$ as substrates.

applications including those of electronics, light-emitting diodes, various light and thermal detectors, etc. In particular, graphene/boron nitride heterolayer has a minimal known lattice mismatch of ≈1.7% and it displays excellent device functionality.[36] Moreover, the magic angle twisting between graphene layers gives rise to superconductivity.[37] Various heterolayered devices including those of excitonic applications, energy storage, display applications, instant sensors for molecules, gas, light, strain, and medical diagnostics are presently being envisaged. Interlayer charge transfers from photonically excited semiconducting layer to the passive layer, hot electron injection from plasmonically exciting layer to the other layer lacking sufficient charge carrier (graphene, for example), second harmonic generation in heterolayers, laser reconfigurable quantum states in heterolayered systems, etc., are recent advances.[38–41] Having successfully established the direct transfer technique of borophene and upon thorough characterizations of its electronic and optical behavior, it was imperative to fabricate heterolayered devices made up of borophene and other 2D materials. The interlayer coupling in borophene-based heterolayers can be determined by interlayer interaction as well as twist angle.

The Hamiltonian for interlayer coupling can be given by[42]

$$U_{\tilde{X}X}\left(\tilde{k},k\right) = -\frac{1}{N}\sum_{G}t_{\tilde{X}X}\left(\tilde{k}+\tilde{G}\right)e^{i\tilde{G}\cdot\tau_{\tilde{X}}}\sum_{R_X}e^{i\left(k-\tilde{k}-\tilde{G}\right)\cdot R_X}$$
$$= -\sum_{G,\tilde{G}}t_{\tilde{X}X}\left(\tilde{k}+G\right)e^{-i\tilde{G}\cdot\tau_X+i\tilde{k}\cdot\tau_{\tilde{X}}}\delta_{k+G,\tilde{k}+\tilde{G}} \quad (1)$$

where Bloch wave vectors are k and $\tilde{k}$ of two layers. Reciprocal lattice vectors are assigned as G and $\tilde{G}$, respectively, R_X is the lattice position vector. The sublattice position vector is τ_X and $\tau_{\tilde{X}}$. $t_{\tilde{X}X}$ is Fourier transform integral.

To have contrast, we selected black phosphorene and MoS_2 as they are p-type and n-type semiconductors, respectively.[43,44] Chemical identification of B/BP and B/MoS_2 heterolayered stacks were done via characteristic Raman fingerprints (see **Figure 6**a,c). Meanwhile, the Raman spectrum of the B/BP heterolayer exhibits peaks of B at 623, 675, 773, 813, 858, 1080, 1124, 1231 cm^{-1} and BP at 357, 457 cm^{-1}, moreover, coupling gives rise to new Raman modes at 214, 532, 938, and 968 cm^{-1} (see Figure 6a, (B, BP, and coupling peaks are marked by peach, cyan, and green color, respectively)). Raman spectrum
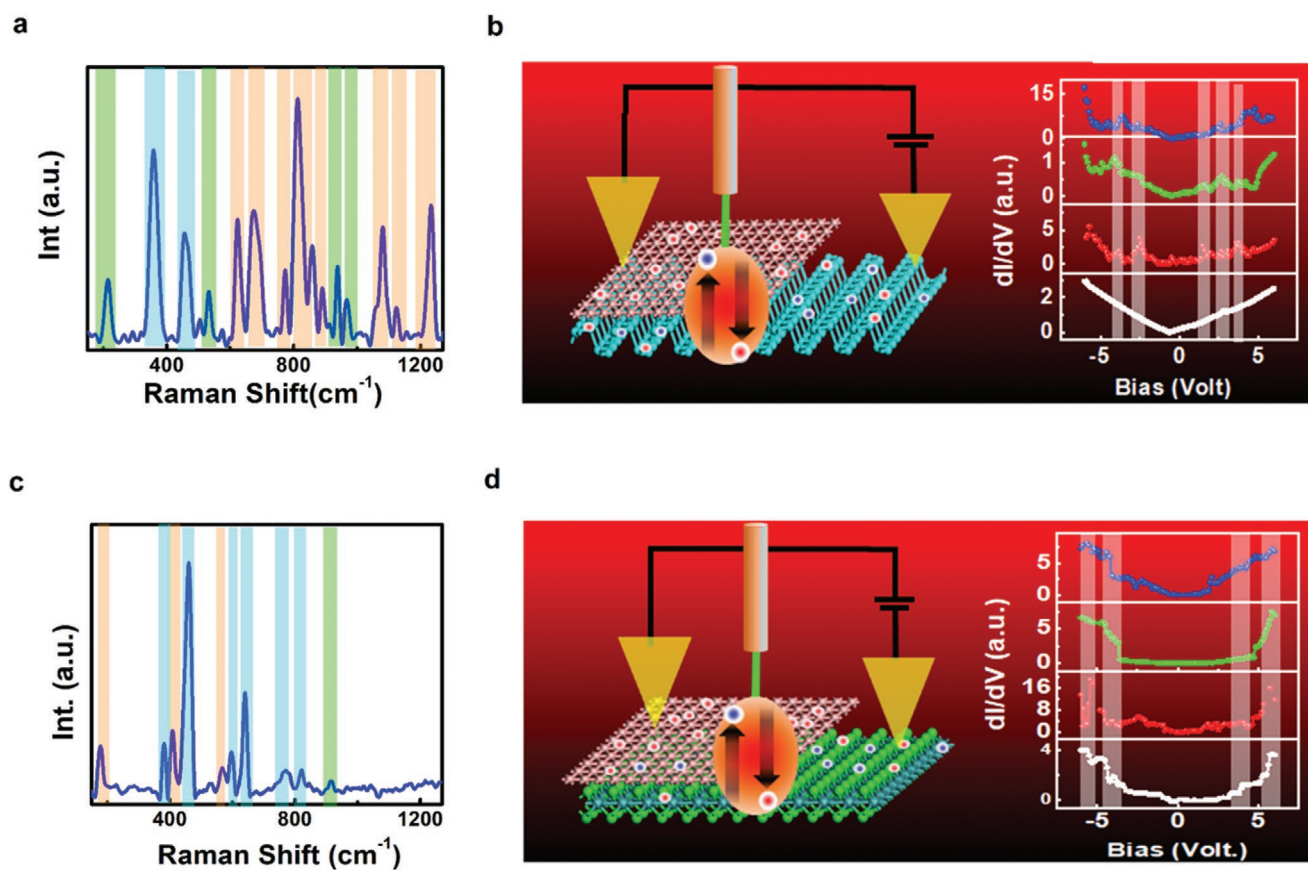
Figure 6. Borophene-based heterolayers with BP and MoS$_2$. a) Raman spectrum of B/BP heterolayer having molecular signatures of both B, BP, and new peaks arising due to interlayer coupling marked by peach, cyan, and green colors. b) Cartoon depicting crystallographic structures of B/BP heterolayer along with differential current (dI/dV) electrical signals. c) Raman spectrum of B/MoS$_2$ heterolayer exhibits peaks of B, MoS$_2$, and new peaks marked by peach, cyan, and green colors. d) Cartoon depicting crystallographic structures of B/MoS$_2$ heterolayer and the corresponding differential current (dI/dV) electrical signals.

of B/MoS$_2$ heterolayer exhibits signature peaks of B at 179, 407, 570 cm^{-1} and MoS$_2$ at 382, 462, 597, 642, 772, 818 cm^{-1} and new Raman modes at 915 cm^{-1} (see Figure 6c, (B, BP, and coupling peaks are marked by peach, cyan, and green color, respectively). Interestingly, we obtained negative photoconductivity in B/BP and positive photoconductivity in B/MoS$_2$ (see Figure S14 in the Supporting Information). Earlier negative photoconductivity has been reported in van der Waals heterolayers.[45] Incident light excites both BP ($E_g \approx 1.8$ eV for monolayer[46]) or MoS$_2$ ($E_g \approx 1.9$ eV for monolayer[47]) and generates excited carriers (electrons and holes) in their respective heterolayers with borophene, however, gets channelized in B/MoS$_2$ where it forms p–n junction which is not true with B/BP, in which case it forms Schottky junction. Moreover, interestingly, we could observe photoexcited quantum states (in differential current signals) at −3.75, −2.44, 1.49, and 3.71 V in B/BP and −5.41, −2.52, 1.81, and 5.65 eV in B/MoS$_2$ heterolayered systems (inset with the schematic diagram of B/BP and B/MoS$_2$ in Figure 6b,d). Such photoexcited coupling quantum states in borophene-based heterolayers obtained in the present research indicate efficient interlayer coupling in heterolayered devices and hint at the excellent potential of borophene-based future generation excitonic devices.

6. Conclusion

A long-awaited breakthrough in the practical realization of borophene down to monolayers at an economic price and simply by exfoliating it from the parent crystal using adhesive tape has been realized. This discovery has crucial importance as it breaks stereotypes of beliefs regarding boron crystal and also for the feasibility of exfoliation. The direct exfoliation technique reported in this article is easy to operate and promises fast fabrication of highly crystalline borophene sheets with enhanced chemical phase purity which are in fact prerequisites for functional devices and sensors. Interestingly, β_{12} and X_3 phases have predominantly been found in 2D crystals, as evident from HRTEM imaging and Raman spectroscopy. It is to be noted that our DFT calculations revealed that borophene needs ≈19.6 meV Å^{-2} (for PBE functional) and 23.6 meV Å^{-2} (for HSE functional) to exfoliate it from its parent crystal, which is higher than those of graphene and BN. Molecular dynamics carried over boron crystal undergoing exfoliation of the top layer due to applied force field suggests that the system loses the potential energy of 23 eV within a period of 70 ps and exfoliated sheet remains intact in crystallinity (β_{12}) and does not disintegrate. To ascertain phase purity of borophene, it was intentionally oxidized

and 2D borophene oxide was found to exhibit altogether distinct behavior, as evident from Raman, XRD, FTIR, and I/V characteristics. It is noteworthy that while borophene oxide electrically behaves as a semiconductor, borophene exhibits a metallic character. It is significant that the borophene-based heterolayered devices having their interface with black phosphorene and MoS$_2$ exhibit photoexcited coupling quantum states, as evident from photoconductive differential current signals. SERS-based molecular detection employing plasmonic metal decorated borophene as an excellent anchor surface has successfully been demonstrated. Experimental realization of micromechanical exfoliation of borophene down to monolayers, establishing its emerging chemical phases and fabrication of borophene-based excitonic heterolayered devices, along with its application in SERS-based molecular sensing, will lead to next-generation devices and functionalities, as is expected.

7. Experimental and Simulation Methods

Exfoliation of Borophene: In the experimental trial, Scotch tape was used to exfoliate borophene; however, it did not yield atomic sheets. It was inferred that the force needed to exfoliate borophene could not be achieved using Scotch tape. As double-sided foam tape (with viscous adhesive polymer) (Brand: Oddy, an Indian company) offered high adhesion to the target surface, therefore, direct micromechanical exfoliation of borophene using double-sided foam tape on an arbitrary substrate was demonstrated. Detailed microscopic and spectroscopic tools were employed to establish the technique.

Double-sided foam tape was first hard-pressed on boron crystal (99.99% pure) (purchased from SMART ELEMENTS GmbH Ferrogasse 4/IA-U80 Wein Germany) using thumb pressing. As a consequence, upon release of pressure, surface layers of crystal were stuck with the tape. Now, the part of the crystal stuck on the tape was subsequently pressed again and again on various locations of the substrate to attain a thinner and thinner layer as an outcome. The division of layers to pristine material and exfoliated sheet was not equal. In fact, the ratio was determined by three forces namely: a) force of adhesion between the tape and boron surface, b) force of cohesion between the top boron surface and underneath boron layer, and c) applied external force. However, the first approximation was that it would make a half–half splitting. With such approximation (which is not exact truth), the final thickness of exfoliated layer after n exfoliation steps was given by

$$t_n = t_0 (1/2)^n \qquad (2)$$

where t_0 is the initial thickness.

Usually, it took 12 to 15 exfoliation attempts to go down to atomic thickness starting from sheets of a few micrometer thickness. The borophene sheets were successfully transferred onto various substrates such as silicon, thermally oxidized silicon (SiO$_2$), and ITO. Transferred material was observed under various microscopy tools such as FESEM, AFM, and TEM. Transferred material was phase characterized by X-ray diffraction, Raman spectroscopy, and X-ray photoelectron spectroscopy. Electronic conductivity of transferred material was carried out by two-probe electrical measurements.

Borophene Oxide: To dig further and differentiate the borophene from its oxide, thermal oxidation of borophene transferred on a thermally oxidized Si substrate was done by heating it on a hot plate at 400 °C for 2 h in the ambient environment and further characterized by Raman, XRD, FTIR, and IV/photoconductivity (PC) measurements.

Heterolayers: The interlayer coupling behavior of B/BP and B/MoS$_2$ heterolayers was investigated. Single crystals of BP and MoS$_2$ were purchased from Sigma-Aldrich with purity 99.995% and 99.99%, respectively. To fabricate heterolayers, the first borophene was transferred onto the substrates using double-sided foam tape and followed by the transfer of BP or MoS$_2$ using their bulk crystals.

Characterization: Various techniques were employed for detailed characterizations of materials. XPS from ESCA+ Omicron nanotechnology GmbH was used to record the XPS signal of borophene in UHV conditions. Confocal Micro-Raman spectrometer (Seki Technotron Corporation, Japan) was adopted in backscattering geometry to record the Raman spectra. He–Ne laser (wavelength 633 nm) worked as an excitation source, and an attached 100× microscope was used to focus and collect the light. TEM and selected-area electron diffraction measurements were carried out using a JEOL JEM 2100 instrument. Morphology investigation and thickness measurements were examined using an atomic force microscope (Agilent 5500) in noncontact mode. A two-probe system having Keithley source-meter (2634 B) and molybdenum pins were utilized for current versus voltage (I–V) and PC measurements in ultrahigh vacuum. Blue, green, and red lasers of wavelength 505, 532, 650 nm were used for optical excitation for photoconductivity measurements. XRD patterns were recorded using a Rigaku TTRX III diffractometer (with Cu-K$_\alpha$ radiation) in the range of 10°–80° at a scan rate of 0.02° min^{-1}. FTIR spectroscopy was done to differentiate the functional group of thermally oxidized borophene using FTIR Shimadzu Irafinity-1.

SERS-Based Molecular Sensing: To investigate SERS capability of borophene, the molecular detection of methylene blue was performed. 10 ppm solution of methylene blue was prepared and for comparative study, it was drop-cast over SiO$_2$, gold-sputtered SiO$_2$ and gold-sputtered borophene were transferred on SiO$_2$ as substrates. A Raman spectrometer having a He–Ne laser (wavelength 633 nm and power ≈ 5 mW) was used for molecule detection.

DFT Calculations: All the electronic structure calculations were performed using the Kohn–Sham DFT,[48] as implemented in the Quantum ESPRESSO package.[49,50] The exfoliation energy of the β_{12}-borophene (from its bulk counterpart) was calculated using a rigorous method recently proposed by Jung et al.[30] According to this method, the exfoliation energy was calculated as the difference between the ground-state energies of the bulk system per layer ($E_{\text{Bulk/layer}}$) and the peeled single-layer ($E_{\text{Single-layer}}$). In the simulations, both the semilocal, PBE,[51,52] and the screened hybrid, HSE,[53] exchange-correlation functionals along with the plane-wave basis sets were used to calculate the exfoliation energies. Here, a 40 Ry kinetic-energy cutoff and a 320 Ry charge-density cutoff were used. Boron atom was represented using an ultrasoft pseudopotential with nonlinear core corrections, namely, B.pbe-n-van_ak.UPF.[54] While using the HSE functional, a $6 \times 6 \times 6$ ($9 \times 9 \times 1$) Monkhorst–Pack[55] k-mesh was used to the integrating the Brillouin zone of the bulk system (single-layer borophene), and with the PBE functional, an $11 \times 11 \times 11$ ($41 \times 41 \times 1$) k-mesh was used for the bulk (single-layer). The dispersion interactions among the layers of β_{12}-borophene were accounted through the Grimme's DFT-D3 correction.[56] Systems were considered to be relaxed when the forces on all the atoms were less than 0.001 Ry Bohr^{-1}.

MD Simulations: Molecular dynamics simulations were conducted using a large-scale atomic/molecular massively parallel simulator package (LAMMPS)[57] to understand the exfoliation of borophene from bulk boron crystals. To investigate the device suitability of borophene integrated into silicon chips, delamination testing was theoretically explored. Hexagonal lattice borophene was used to perform MD calculations. The simulation setup consisting of multilayer borophene and silicon was modeled using VESTA.[58] Two configurations were considered for analysis. Force was applied to the top layer to be exfoliated in the Z-direction until the layer detached from the bulk material and potential energy was calculated for the different configurations. Periodic boundary conditions were imposed in the X- and Y-directions. The force-field interactions between borophene atoms were defined using the empirical Stillinger–Weber potential[59] which contained the following two-body and three-body interactions terms

$$V2 = \varepsilon A (B\sigma^p r_{ij}^{-q} - \sigma^q r_{ij}^{-q}) \exp[\sigma(r_{ij} - a\sigma)^{-1}] \qquad (3)$$

**ADVANCED
SCIENCE NEWS**

www.advancedsciencenews.com

**ADVANCED
MATERIALS**

www.advmat.de

and

$$V3 = \varepsilon\lambda \exp[\gamma\sigma(r_{ij} - a\sigma)^{-1} + \gamma\sigma(r_{jk} - a\sigma)^{-1}](\cos q_{jik} - \cos q_0)^2 \quad (4)$$

where, r is the distance between atoms and θ is the angle formed by the bonds (θ_0 is the equilibrium bond angle). The system was equilibrated via a Nose–Hoover thermostat and the energy of the system was minimized using force and energy tolerance of 1×10^{-10} kcal mol^{-1}.

Supporting Information

Supporting Information is available from the Wiley Online Library or from the author.

Conflict of Interest

The authors declare no conflict of interest.

Author Contributions

S.C., P.R., and M.M. contributed equally to this work. P.K. and G.J.C. conceived the idea. D.J.L. helped with boron crystals and was part of preliminary discussions. S.C. and P.R. exfoliated and transferred borophene and other 2D crystals onto substrates. S.C. carried out detailed characterizations of exfoliated materials and explored applications. P.R. carried out layer-dependent Raman spectroscopy under the guidance of E.H.S.S. M.M. carried out molecular dynamics simulation under the supervision of G.J.C. S.S.R.K.C.Y. carried out DFT-based calculations of exfoliation energy. S.C.,P.K., M.M., and G.J.C. wrote the paper together. The project was overall supervised by P.K. and G.J.C.

Data Availability Statement

Research data are not shared.

[1] L. Burnelle, J. J. Kaufmann, *J. Chem. Phys.* **1965**, *43*, 3540.
[2] A. J. Mannix, Z. Zhang, N. P. Guisinger, B. I. Yakobson, M. C. Hersam, *Nat. Nanotechnol.* **2018**, *13*, 444.
[3] X. Sun, X. Liu, J. Yin, J. Yu, Y. Li, Y. Hang, X. Zhou, M. Yu, J. Li, G. Tai, W. Guo, *Adv. Funct. Mater.* **2017**, *27*, 1603300.
[4] A.de Falin, Q. Cai, E. J. G. Santos, D. Scullion, D. Qian, R. Zhang, Z. Yang, S. Huang, K. Watanabe, T. Taniguchi, M. R. Barnett, Y. Chen, R. S. Ruoff, L. H. Li, *Nat. Commun.* **2017**, *8*, 15815.
[5] K. S. Novoselov, A. K. Geim, S. V. Morozov, D. Jiang, Y. Zhang, S. V. Dubonos, I. V. Grigorieva, A. A. Firsov, *Science* **2004**, *306*, 666.
[6] A. K. Geim, K. S. Novoselov, *Nat. Mater.* **2007**, *6*, 183.
[7] Y. Yin, Z. Cheng, L. Wang, *Sci. Rep.* **2015**, *4*, 5758.
[8] P. Ranjan, J. M. Lee, P. Kumar, A. Vinu, *Adv. Mater.* **2020**, *32*, 2000531.
[9] Z. Wang, T. Lü, H. Wang, Y. P. Feng, J. C. Zheng, *Front. Phys.* **2019**, *14*, 33403.
[10] K. I. Bolotin, K. J. Sikes, Z. Jiang, M. Klima, G. Fudenberg, J. Hone, P. Kim, H. L. Stormer, *Solid State Commun.* **2008**, *146*, 351.
[11] B. W. H. Baugher, H. O. H. Churchill, Y. Yang, P. J. Herrero, *Nano Lett.* **2013**, *13*, 4212.
[12] L. Li, Y. Yu, G. Ye, X. Ou, H. Wu, D. Feng, X. H. Chen, Y. Zhang, *Nat. Nanotechnol.* **2014**, *9*, 372.
[13] L. Li, M. Engel, D. B. Farmer, S. J. Han, H. S. Wong, *ACS Nano* **2016**, *10*, 4672.
[14] S. Tomar, P. Rastogi, B. S. Bhadoria, S. Bhowmick, A. Agarwal, S. Y. Chauhan, in *2018 IEEE Int. Conf. on Electronics, Computing and Communication Technologies (CONECCT)*, IEEE, Piscataway, NJ, USA **2018**, https://doi.org/10.1109/CONECCT.2018.8482369.
[15] C. L. Zou, D. Q. Guo, F. Zhang, J. Meng, H. L. Miao, W. Jiang, *Phys. E* **2018**, *104*, 138.
[16] Y. Zhao, J. Qiao, Z. Yu, P. Yu, K. Xu, S. P. Lau, W. Zhou, Z. Liu, X. Wang, Y. Ji, Y. Chai, *Adv. Mater.* **2017**, *29*, 1604230.
[17] A. J. Mannix, X. F. Zhou, B. Kiraly, J. D. Wood, D. Alducin, B. D. Myers, X. Liu, B. L. Fisher, U. Santiago, J. R. Guest, M. J. Yacaman, A. Ponce, A. R. Oganov, M. C. Hersam, N. P. Guisinger, *Science* **2015**, *350*, 1513.
[18] B. Feng, J. Zhang, Q. Zhong, W. Li, S. Li, H. Li, P. Cheng, S. Meng, L. Chen, K. Wu, *Nat. Chem.* **2016**, *8*, 563.
[19] Q. Zhong, J. Zhang, P. Cheng, B. Feng, W. Li, S. Sheng, H. Li, S. Meng, L. Chen, K. Wu, *J. Phys.: Condens. Matter* **2017**, *29*, 095002.
[20] R. Wu, A. Gozar, I. Božović, *npj Quantum Mater.* **2019**, *4*, 40.
[21] P. Ranjan, T. K. Sahu, R. Bhushan, S. S. Yamijala, D. J. late, P. Kumar, A. Vinu, *Adv. Mater.* **2019**, *31*, 1900353.
[22] H. Li, L. Jing, W. Liu, J. Lin, R. Y. Tay, S. H. Tsang, E. H. T. Teo, *ACS Nano* **2018**, *12*, 1262.
[23] F. Zhang, L. She, C. Jia, X. He, Q. Li, J. Sun, Z. Lei, Z. Liu, *RSC Adv.* **2020**, *10*, 27532.
[24] S. Sheng, J. Wu, C. Xin, Q. Zhong, W. Li, W. Hu, J. Gou, P. Cheng, P. Tan, L. Chen, K. Wu, *ACS Nano* **2019**, *13*, 4133.
[25] A. P. Sergeeva, I. A. Popov, Z. A. Piazza, W. L. Li, C. Romanescu, L. S. Wang, A. I. Boldyrev, *Acc. Chem. Res.* **2014**, *47*, 1349.
[26] H. G. Lu, Y. B. Wu, Y. W. Mu, G. F. Wei, Z. P. Liu, J. Li, S. Li, L. S. Wang, *Nat. Chem.* **2014**, *6*, 175.
[27] H. Tang, S. Ismail-Beigi, *Phys. Rev. Lett.* **2007**, *99*, 115501.
[28] B. Albert, H. Hillebrecht, *Angew. Chem., Int. Ed.* **2009**, *48*, 8640.
[29] X. Wu, J. Dai, Y. Zhao, Z. Zhuo, J. Yang, X. C. Zeng, *ACS Nano* **2012**, *6*, 7443.
[30] J. H. Jung, C.-H. Park, J. Ihm, *Nano Lett.* **2018**, *18*, 2759.
[31] P. Manimunda, Y. Nakanishi, Y. M. Jaques, S. Susarla, C. F. Woellner, S. Bhowmick, S. A. S. Asif, D. S. Galvão, C. S. Tiwary, P. M. Ajayan, *2D Mater.* **2017**, *4*, 045005.
[32] N. Levy, S. A. Burke, K. L. Meaker, M. Panlasigui, A. Zettl, F. Guinea, A. H. C. Neto, M. F. Crommie, *Science* **2010**, *329*, 544.
[33] M. Motlag, P. Kumar, K. Y. Hu, S. Jin, J. Li, J. Shao, X. Yi, Y. H. Lin, J. C. Walrath, L. Tong, X. Huang, R. S. Goldman, L. Ye, G. J. Cheng, *Adv. Mater.* **2019**, *31*, 1900597.
[34] R. Zhang, Z. Li, J. Yang, *J. Phys. Chem. Lett.* **2017**, *8*, 4347.

[35] L. Yan, P. Liu, H. Li, Y. Tang, J. He, X. Huang, B. Wang, L. Zhou, *npj Comput. Mater.* **2020**, *6*, 94.

[36] J. Xue, S. Yamagishi, D. Bulmash, P. Jacquod, A. Deshpande, K. Watanabe, T. Taniguchi, P. J. Herrero, B. J. LeRoy, *Nat. Mater.* **2011**, *10*, 282.

[37] Y. Cao, V. Fatemi, S. Fang, K. Watanabe, T. Taniguchi, E. Kaxiras, P. J. Herrero, *Nature* **2018**, *556*, 43.

[38] A. Pant, Z. Mutlu, D. Wickramaratne, H. Cai, R. K. Lake, C. Ozkan, S. Tongay, *Nanoscale* **2016**, *8*, 3870.

[39] W. Kim, J. Y. Ahn, J. Oh, J. H. Shim, S. Ryu, *Nano Lett.* **2020**, *20*, 8825.

[40] A. Vargas, F. Liu, C. Lane, D. Rubin, S. Bilgin, Z. Hennighausen, M. DeCapua, A. Bansil, S. Kar, *Sci. Adv.* **2017**, *3*, e1601741.

[41] J. I. A. Li, Q. Shi, Y. Zeng, K. Watanabe, T. Taniguchi, J. Hone, C. R. Dean, *Nat. Phys.* **2019**, *15*, 898.

[42] M. Koshino, *New J. Phys.* **2015**, *17*, 015014.

[43] H. Liu, Y. Du, Y. Deng, P. D. Ye, *Chem. Soc. Rev.* **2014**, *44*, 2732.

[44] O. V. Yazyev, A. Kis, *Mater. Today* **2015**, *18*, 20.

[45] Y. Wang, E. Liu, A. Gao, T. Cao, M. Long, C. Pan, L. Zhang, J. Zeng, C. Wang, W. Hu, S. J. Liang, F. Miao, *ACS Nano* **2018**, *12*, 9513.

[46] K. Cho, J. Yang, Y. Lu, *J. Mater. Res.* **2017**, *32*, 2839.

[47] H. J. Conley, B. Wang, J. I. Ziegler, R. F. Haglund, J. S. T. Antelides, K. I. Bolotin, *Nano Lett.* **2013**, *8*, 3626.

[48] P. Hohenberg, W. Kohn, *Phys. Rev. B* **1964**, *136*, B864.

[49] P. Giannozzi, S. Baroni, N. Bonini, M. Calandra, R. Car, C. Cavazzoni, D. Ceresoli, G. L. Chiarotti, M. Cococcioni, I. Dabo, A. Dal Corso, S. de Gironcoli, S. Fabris, G. Fratesi, R. Gebauer, U. Gerstmann, C. Gougoussis, A. Kokalj, M. Lazzeri, L. Martin-Samos, N. Marzari, F. Mauri, R. Mazzarello, S. Paolini, A. Pasquarello, L. Paulatto, C. Sbraccia, S. Scandolo, G. Sclauzero, A. P. Seitsonen, A. Smogunov, P. Umari, R. M. Wentzcovitch, *J. Phys.: Condens. Matter* **2009**, *21*, 395502.

[50] P. Giannozzi, O. Andreussi, T. Brumme, O. Bunau, M. Buongiorno Nardelli, M. Calandra, R. Car, C. Cavazzoni, D. Ceresoli, M. Cococcioni, N. Colonna, I. Carnimeo, A. Dal Corso, S. de Gironcoli, P. Delugas, R. A. Distasio, A. Ferretti, A. Floris, G. Fratesi, G. Fugallo, R. Gebauer, U. Gerstmann, F. Giustino, T. Gorni, J. Jia, M. Kawamura, H.-Y. Ko, A. Kokalj, E. Küçükbenli, M. Lazzeri, M. Marsili, N. Marzari, F. Mauri, N. L. Nguyen, H.-V. Nguyen, A. Otero-de-la-Roza, L. Paulatto, S. Poncé, D. Rocca, R. Sabatini, B. Santra, M. Schlipf, A. P. Seitsonen, A. Smogunov, I. Timrov, T. Thonhauser, P. Umari, N. Vast, X. Wu, S. Baroni, *J. Phys.: Condens. Matter* **2017**, *29*, 465901.

[51] J. P. Perdew, K. Burke, M. Ernzerhof, *Phys. Rev. Lett.* **1996**, *77*, 3865.

[52] Y. Zhang, W. Yang, *Phys. Rev. Lett.* **1998**, *80*, 890.

[53] A. V. Krukau, O. A. Vydrov, A. F. Izmaylov, G. E. Scuseria, *J. Chem. Phys.* **2006**, *125*, 224106.

[54] S. Baroni, N. Bonini, M. Calandra, R. Car, C. Cavazzoni, D. Ceresoli, G. L. Chiarotti, M. Cococcioni, I. Dabo, A. Dal Corso, S. de Gironcoli, S. Fabris, G. Fratesi, R. Gebauer, U. Gerstmann, C. Gougoussis, A. Kokalj, M. Lazzeri, L. Martin-Samos, N. Marzari, F. Mauri, R. Mazzarello, S. Paolini, A. Pasquarello, L. Paulatto, C. Sbraccia, S. Scandolo, G. Sclauzero, A. P. Seitsonen, A. Smogunov, P. Umari, R. M. Wentzcovitch, *J. Phys.: Condens. Matter* **2009**, *21*, 395502.

[55] H. J. Monkhorst, J. D. Pack, *Phys. Rev. B.* **1976**, *13*, 5188.

[56] S. Grimme, J. Antony, S. Ehrlich, H. Krieg, *J. Chem. Phys.* **2010**, *132*, 154104.

[57] S. Plimpton, *Fast Parallel Algorithms for Short-Range Molecular Dynamics*, Sandia National Labs, Albuquerque, NM, USA **1993**.

[58] K. Momma, F. Izumi, *J. Appl. Crystallogr.* **2008**, *41*, 653.

[59] Y.-P. Zhou, J.-W. Jiang, *Sci. Rep.* **2017**, *7*, 45516.

2102039 (13 of 13)